DOI: 10.1002/ejic.200601023

Correlation between the Stoichiometry and the Bistability of Electronic States in Valence-Tautomeric $Rb_xMn[Fe(CN)_6]_y \cdot zH_2O$ Complexes

Saioa Cobo,[a] Raquel Fernández,[a] Lionel Salmon,[a] Gábor Molnár,[a] and Azzedine Bousseksou*[a]

Keywords: Prussian blue analogues / Magnetic properties / Phase transitions / Raman spectroscopy

A series of Prussian blue analogues, $Rb_xMn[Fe(CN)_6]_y \cdot zH_2O$ with different stoichiometries have been synthesized. Elemental analyses reveal a quasilinear decrease in *x* and *y* when *z* increases. Some of these samples present a first-order phase transition between the Mn^{II}–Fe^{III} and Mn^{III}–Fe^{II} electronic states with large thermal hysteresis loops observed in the magnetic susceptibility. The phase-transition temperatures correlate with the stoichiometry, but quantitative predictions cannot be made because of the disordered nature of the compounds. Contrary to previous literature reports, calorimetric and Raman spectroscopic measurements reveal that the charge-transfer phase transition is accompanied by a significant entropy change, $\Delta S = 48–59\ J\,K^{-1}\,mol^{-1}$, of mainly vibrational origin. In addition to the thermal phase transition, Raman spectra also show that below ca. 120 K a photoinduced Mn^{III}–Fe^{II} to Mn^{II}–Fe^{III} conversion occurs in certain stoichiometries.

Introduction

The bistability of electronic states in transition-metal complexes represents an important field of research in coordination chemistry. The bistability in these compounds generally arises from strong electron-lattice couplings. Typical examples are spin crossover phenomena,[1,2] and valence-tautomerism.[3] In this latter class, valence-tautomeric Prussian blue analogues of transition metals with general formula $A_xM^{II}[M'^{III}(CN)_6]_y \cdot nH_2O$ (where A is an alkali metal cation, and M and M′ are divalent or trivalent transition-metal cations) have attracted considerable interest because of their remarkable magnetic properties, such as high Curie temperatures[4,5] or photomagnetic phenomena.[6–8] In some of these complexes, a first-order thermal phase transition was observed and associated with metal-to-metal electron transfer.[9,10] The compound $Rb_xMn[Fe(CN)_6]_y \cdot zH_2O$ shown in Figure 1 (noncoordinated water molecules and rubidium atoms are not represented) is one of the most studied members of this family.[10,11] It exhibits switching phenomena between the high-temperature (HT) Fe^{III}(S = 1/2)–CN–Mn^{II}(S = 5/2) and the low-temperature (LT) Fe^{II}(S = 0)–CN–Mn^{III}(S = 2) states that can be induced by changing the sample temperature or pressure as well as by light irradiation.[10–18] The two phases display markedly different magnetic, optical, and electric properties.

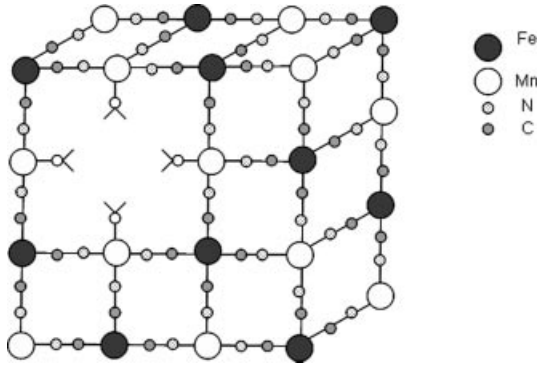

Figure 1. Schematic structure of $Rb_xMn[Fe(CN)_6]_y \cdot zH_2O$ with a $Fe(CN)_6^{3-}$ vacancy. (Noncoordinated water molecules and rubidium atoms are not represented.)

Even if $Rb_xMn[Fe(CN)_6]_y \cdot zH_2O$ has been the object of many investigations, several questions remain to be clarified. Notably, the control of the phase-transition temperature is an important issue because these compounds present very large thermal hysteresis loops (up to 138 K).[18] Such a large bistability domain is an appealing property for the application of these materials in various devices (e.g. memories). In preliminary results, Ohkoshi et al.[17] found a correlation between the hysteresis width and the stoichiometry of these compounds, but further measurements performed by the same group[18] and others[11] appear to escape this correlation. Another important question concerns the origin of the thermal phase transition. This question has been investigated extensively in the case of spin-crossover complexes and it is now generally accepted that thermal spin

[a] Laboratoire de Chimie de Coordination, CNRS UPR-8241, 205 Route de Narbonne, 31077 Toulouse, France
Fax: +33-561-553-003
E-mail: boussek@lcc-toulouse.fr

crossover is an entropy-driven phenomenon and coupling between the electronic states and the phonon system plays a fundamental role.[19] Data on Prussian blue analogues are considerably less extensive.[20] However, it seems a reasonable assumption to attribute a similar importance to the vibrations because the most prominent structural changes in both cases are the metal–ligand bond length. Therefore, it is very surprising that the transition entropy for the title compound was found hardly of the order of the electronic entropy change.[10,21] This paper has been written in order to discuss these questions. In this aim, we have synthesized nine samples of different stoichiometry and characterized them by using Raman spectroscopy, elemental analysis, and magnetic and calorimetric measurements.

Results and Discussion

Stoichiometry and Magnetic Properties

Elemental analysis reveals significant differences between the different $Rb_xMn[Fe(CN)_6]_y{\cdot}zH_2O$ samples. For each compound, a chemical formula, taking into account the chemical arrangement of the system, the weight percentage of each element, and the electroneutrality, is proposed (Table 1). Figure 2 shows the Rb^+ (x) and H_2O (z) content of each sample and those reported in refs.[11,17] as a function of the iron proportion. Clearly, independent of the synthetic method, a quasilinear correlation exists between these quantities, which can be understood as follows. In each case, the system contains a certain amount of $[Fe(CN)_6]^{3-}$ vacancies (Figure 1). The formation of these vacancies leads to a lower Rb^+ proportion (x) in order to maintain the charge neutrality. Indeed, the regression analysis shows that for each missing $[Fe(CN)_6]^{3-}$ unit, ca. three Rb^+ ions are removed from the crystal lattice. Moreover, the H_2O content (z) increases because the water molecules complete the coordination around the Mn^{II} ions at the place of the missing $[Fe(CN)_6]^{3-}$ entities and we can safely state that the non-stoichiometric crystal lattice contains a relatively large amount of noncoordinated water molecules as well. However, according to Figure 2b, the formation of one $[Fe(CN)_6]^{3-}$ vacancy leads to the uptake of ca. 22 water molecules; 6 of which would complete the coordination sphere of the Mn^{II} ions at the place of the missing N atoms, and the remaining water molecules become encapsulated in the remaining cavities. Let us also note that the reproducibility of the synthesis (samples **7**–**9**) is relatively poor owing mainly to the extreme insolubility and the disordered nature of the sample.

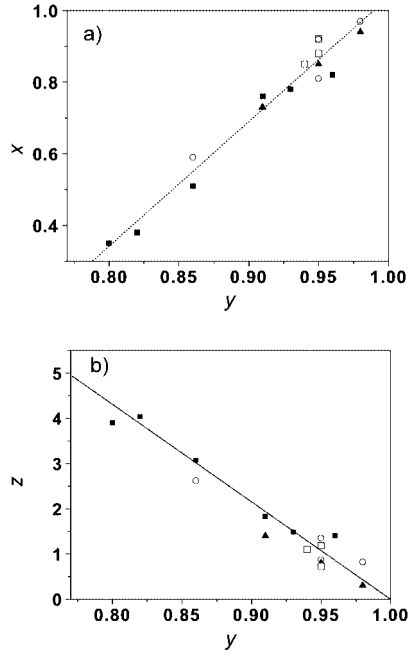

Figure 2. Rb^+ content (a) and H_2O content (b) as a function of Fe content in $Rb_xMn[Fe(CN)_6]_y{\cdot}zH_2O$. (Full squares: samples **1**–**6**, open squares: samples **7**–**9**, open circles: data from ref.,[11] full triangles: data from ref.[17]) Straight lines represent linear fits on the data.

Table 1. Elemental analysis data and proposed formula for the different samples.

Sample		C	N	Mn	Fe	Rb	Proposed formula
1	Observed	18.19	20.80	16.78	13.71	9.12	$Rb_{0.35}Mn[Fe(CN)_6]_{0.80}{\cdot}3.90H_2O$
	Calculated	17.57	20.5	16.78	13.63	9.12	
2	Observed	18.19	20.82	16.24	13.51	9.80	$Rb_{0.38}Mn[Fe(CN)_6]_{0.82}{\cdot}4.04H_2O$
	Calculated	17.49	20.4	16.24	13.55	9.61	
3	Observed	18.62	21.34	16.37	14.33	12.88	$Rb_{0.51}Mn[Fe(CN)_6]_{0.86}{\cdot}3.07H_2O$
	Calculated	18.46	21.53	16.37	14.31	12.99	
4	Observed	19.26	22.06	15.83	14.66	18.70	$Rb_{0.76}Mn[Fe(CN)_6]_{0.91}{\cdot}1.83H_2O$
	Calculated	18.87	22.02	15.83	14.63	18.71	
5	Observed	19.62	22.55	15.80	15.04	19.30	$Rb_{0.78}Mn[Fe(CN)_6]_{0.93}{\cdot}1.48H_2O$
	Calculated	19.29	22.5	15.8	14.96	19.2	
6	Observed	19.60	22.49	15.63	15.18	19.90	$Rb_{0.82}Mn[Fe(CN)_6]_{0.96}{\cdot}1.40H_2O$
	Calculated	19.64	22.91	15.63	15.22	19.9	
7	Observed	19.6	22.6	15.2	16.0	21.1	$Rb_{0.85}Mn[Fe(CN)_6]_{0.94}{\cdot}1.10H_2O$
	Calculated	19.7	22.9	15.2	15.3	21.1	
8	Observed	19.9	22.5	15.5	15.0	21.1	$Rb_{0.88}Mn[Fe(CN)_6]_{0.95}{\cdot}1.18H_2O$
	Calculated	19.3	22.5	15.5	15.0	21.2	
9	Observed	19.8	22.8	15.8	15.4	22.5	$Rb_{0.92}Mn[Fe(CN)_6]_{0.95}{\cdot}0.72H_2O$
	Calculated	19.6	22.9	15.8	15.2	22.6	

Figure 3 shows the product of molar magnetic susceptibility and the temperature for samples **1**–**9** as a function of temperature. One of the interesting points of the $\chi_M T$–T plots is that the values for compounds **1**–**3** are around 5.0 $cm^3 mol^{-1}$ K for the whole range of temperatures, which indicates that the ground state consists mainly of the $Fe^{III}{}_{LS}$–CN–$Mn^{II}{}_{HS}$ configuration (HT phase). In contrast, the $\chi_M T$ value for compounds **4**–**6** and **7**–**9** varies significantly with the temperature and reveals a HT→LT phase transition with a large hysteresis loop. We can explain these results by using the arguments proposed for the first time in ref.[11] In the idealized formula Rb:Mn:Fe = 1:1:1 for $Rb_xMn[Fe(CN)_6]_y \cdot zH_2O$, the ground state is the $Fe^{II}{}_{LS}$–CN–$Mn^{III}{}_{HS}$ configuration, which remains stable up to ca. 300 K. Above this temperature, the $Fe^{III}{}_{LS}$–CN–$Mn^{II}{}_{HS}$ configuration becomes the thermodynamically stable phase because of its higher entropy (vide infra). On the contrary, in a nonidealized formula with vacant $Fe(CN)_6$ sites, oxygen atoms of the water molecule coordinate to the Mn ions instead of the nitrogen atoms of the cyanide, and the average environment of the manganese ions changes to $Mn^{III}(O_2H)_x(NC)_{6-x}$. As a result, the ligand field strength of the Mn^{III} ions becomes weaker and consequently the redox potential of the Mn^{III}/Mn^{II} couple increases leading finally to the oxidation of the Fe^{II} ion. If the water content is sufficiently high, the redox potential increases to such an extent that the $Fe^{III}{}_{LS}$–CN–$Mn^{II}{}_{HS}$ form becomes stable at very low temperatures.

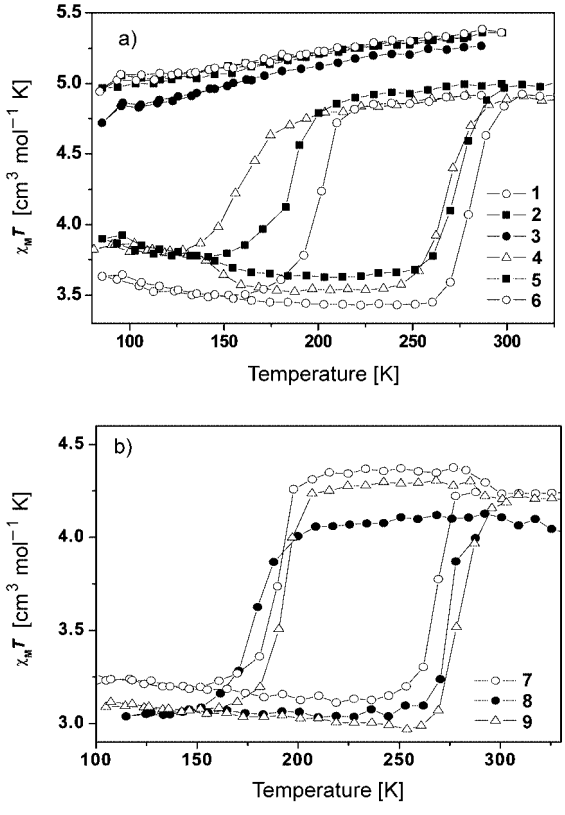

Figure 3. $\chi_M T$ versus T curves for samples **1**–**6** (a) and **7**–**9** (b). (Data points are connected to guide the eye.)

The $\chi_M T$–T curve for compound **4** decreases abruptly from 4.7 $cm^3 mol^{-1}$ K to 3.6 $cm^3 mol^{-1}$ K below 184 K upon cooling and, conversely, as the sample was warmed in the LT phase, the $\chi_M T$ value increased around 272 K and reached the HT value. The width of the thermal hysteresis loop (112 K) is defined by $T_{1/2}\downarrow$ = 160 K and $T_{1/2}\uparrow$ = 272 K. The $\chi_M T$–T plots for sample **6** showed ΔT = 81 K, $T_{1/2}\downarrow$ = 201 K, $T_{1/2}\uparrow$ = 282 K, and for sample **5** ΔT = 87 K, $T_{1/2}\downarrow$ = 184 K, $T_{1/2}\uparrow$ = 271 K. This series of compounds agrees with Ohkoshi's proposition,[17] that is, the ΔT value increases as the Fe/Mn ratio decreases. To prove the reproducibility of the synthesis, and Ohkoshi's findings, we have synthesized three more compounds, **7**–**9**. Figure 4 shows the ΔT, $T_{1/2}\downarrow$, and $T_{1/2}\uparrow$ values for each sample and for those reported in refs.[11,17] as a function of the Rb^+ proportion (although the relevant parameter is the Fe content, we have chosen to plot them as a function of the Rb content because [Fe] and [Rb] are proportional and the sample-to-sample changes in [Rb] are higher). This figure appears to indeed reveal some general trends. When decreasing the value of x (i.e. the Rb content) from 0.97 to 0.73, the phase transition shifts from 301 K (240 K) to

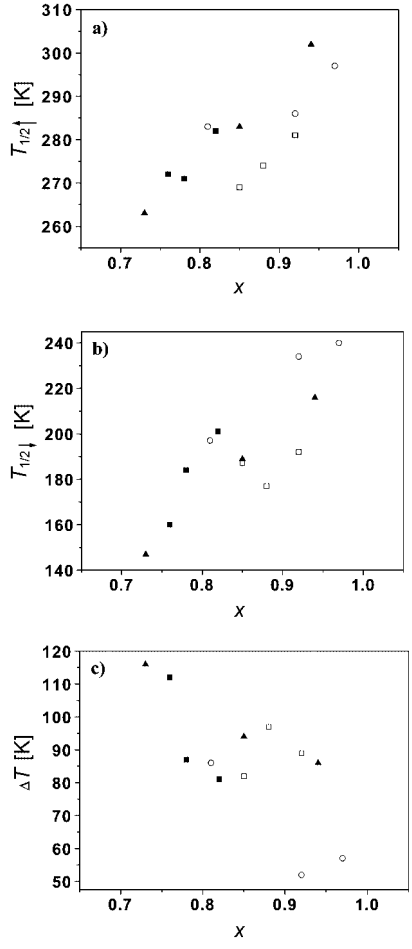

Figure 4. Phase transition temperatures in the heating (a) and cooling (b) modes and hysteresis width (c) as a function of the Rb content in $Rb_xMn[Fe(CN)_6]_y \cdot zH_2O$. (Full squares: samples **1**–**6**, open squares: samples **7**–**9**, open circles: data from ref.,[11] full triangles: data from ref.[17])

263 K (147 K) in the heating (cooling) cycles, and accordingly the hysteresis width increases. It is interesting to note that the increase in the hysteresis width is due to the fact that $T_{1/2}\downarrow$ changes more than $T_{1/2}\uparrow$. In fact, according to the Ising-like model developed in ref.,[22] the hysteresis loop width is proportional to J/T_c, where J is a phenomenological parameter for the cooperativity and T_c is the transition temperature. Because $T_c \cong (T_{1/2}\downarrow + T_{1/2}\uparrow)/2$, this inverse proportional relationship explains the increase in the hysteresis width when $T_{1/2}\downarrow$ decreases.

Nonetheless, the data are rather scattered and one can observe differences as much as 20–30 K for samples having the same composition. Let us also note that the sample reported in ref.,[18] which contains also an important amount of the reduced form, Fe^{II}–CN–Mn^{II} escapes even the loose correlation seen in Figure 4. In summary, however, we find that the general tendency is the shift in the phase transition to lower temperatures with increasing deviations from the idealized (Rb:Mn:Fe = 1:1:1) stoichiometry. As explained above, this observation can be understood as a result of the weakening ligand field on the manganese ions and associated change of the redox properties. We believe that the fact that the correlation is rather vague is a result of the disordered nature of these compounds containing various types of defects in arbitrary distribution.

Entropy Change on Phase Transition

As already mentioned, the valence-tautomeric thermal phase transition is entropy driven. The entropy change can be represented as the sum of electronic, vibrational, configurational, rotational, and translational terms. The two latter are excluded from consideration in the solid state. Moreover, in the absence of orientational disorder the configurational term can also be neglected. The electronic term may contain spin and orbital contributions. Assuming the idealized cubic symmetry of the Prussian blue structure, the LT phase [$Mn^{III}(^5E_g$)–$Fe^{II}(^1A_{1g})$] has a 2(orbital) × 5(spin) = 10-fold degeneracy, whereas the degeneracy of the HT phase [$Mn^{II}(^6A_{1g}$)–$Fe^{III}(^2T_{2g})$] is 3(orbital) × 12(spin) = 36-fold. This would lead to an electronic entropy change of $\Delta S_{el} = R\ln(36/10) = 10.6\ J\,K^{-1}\,mol^{-1}$. However, the orbital degeneracy of the Mn^{III} ion is removed by the Jahn–Teller effect[10] and it is reasonable to assume also that in the non-stoichiometric disordered structures, the local symmetry around the iron atoms are not perfectly octahedral either, and therefore, the orbital moment of the Fe^{III} ion is quenched, which leads to the $^5B_{1g}$ and $^2B_{2g}$ terms for Mn^{III} and Fe^{III}, respectively. Then, one obtains the spin-only value of $\Delta S_{el} = R\ln(12/5) = 7.3\ J\,K^{-1}\,mol^{-1}$. This value is indeed quite close to the experimentally observed value of $6\ J\,K^{-1}\,mol^{-1}$.[10] However, it is well-known that the weakening of the metal–ligand bonds results in a strong increase in the vibrational partition functions.[23] In the case of $Rb_xMn[Fe(CN)_6]_y{\cdot}zH_2O$, the formation of the LT phase is accompanied by a discontinuous lattice contraction of ca. 10% and a reduction in the average Fe–Mn distance from 5.27 Å to 5.10 Å! Such a huge change in the bond lengths must lead to observable differences in the vibrational entropy. For this reason, we have carried out DSC measurements. Figure 5 shows the DSC curves of sample **7**, which exhibits singularities around 170 K and 280 K in the cooling and heating modes, respectively. These peaks clearly correspond to the charge-transfer phase transition. The enthalpy variation associated with the phase transition is $\Delta H = 11\ kJ\,mol^{-1}$. Then, assuming that $T_c \cong (T_{1/2}\downarrow + T_{1/2}\uparrow)/2 = 230$ K (calculated from the more accurate magnetic data), one obtains $\Delta S = \Delta H/T_c = 48\ J\,K^{-1}\,mol^{-1}$. Fairly similar results ($\Delta H = 13.6\ kJ\,mol^{-1}$, $\Delta S = 59\ J\,K^{-1}\,mol^{-1}$) were obtained for sample **6** as well, whereas sample **2**, which remains in the HT phase in the whole temperature range, showed no singularity in the calorimetric data. These results are therefore in significant disagreement with the results of other groups,[10,11] but seem to be more realistic for us taking into account the electronic and structural changes discussed above.

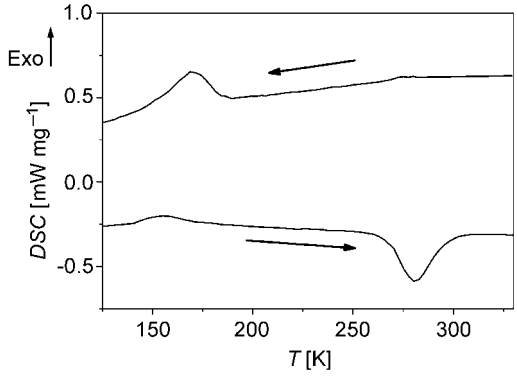

Figure 5. DSC curves of sample **7** in the heating and cooling cycles.

The calorimetric data strongly suggest that the phase transition is associated with a significant change in the vibrational entropy (ca. 40–50 $J\,K^{-1}\,mol^{-1}$), which should be obviously reflected by the vibrational spectra of the compound. Representative Raman spectra of **7** are shown in Figure 6. In agreement with previous IR spectroscopic data on this complex,[12] the CN stretching modes can be chosen to follow the electron transfer. In the HT phase, two intense Raman modes were observed around 2159 and 2170 cm^{-1} and assigned to the stretching modes of the CN moiety bridged between Fe^{III} and Mn^{II}. It should be also noted that the completely reduced form Fe^{II}–CN–Mn^{II} of the compound was not observed in the Raman spectra. When decreasing the temperature, the spectra change drastically and at 120 K, two Raman modes are observed at ca. 2096 and 2114 cm^{-1}, which can be assigned to the stretching modes of the CN ligand linked to the Fe^{II} and Mn^{III} in the LT phase. The phase transition appears to be incomplete at low temperatures. CN stretching modes thus provide very useful diagnostic features concerning the electronic configuration of the system, but their contribution to the vibrational entropy is negligible as only the frequencies below ca. 600 cm^{-1} can give significant contributions.[23] Low frequency Raman spectra in the two phases are shown in Fig-

ure 6b. Without isotope-substitution data, the assignment of these modes is not feasible, but we note that, according to literature data,[24] frequencies around 550, 450, and 200 cm^{-1} in Prussian blue analogues can be attributed to ν(FeC), δ(FeCN), and δ(CFeC) modes, respectively. Indeed, a number of modes appear around these frequencies. Although the former do not seem to be very sensitive to the actual electronic configuration, huge changes are observed at lower frequencies (180–320 cm^{-1}), which thus tend to support the large vibrational entropy changes revealed by the calorimetry data.

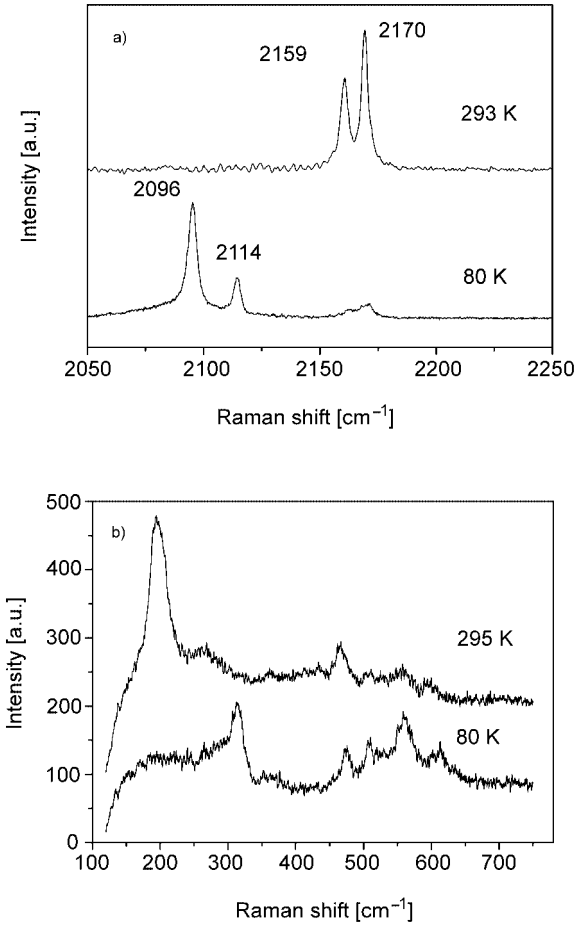

Figure 6. Raman spectra of sample **7** in the ν_{CN} (a) and low-frequency (b) regions at selected temperatures (cooling mode).

Additional Raman Spectroscopic Data

During the Raman spectroscopic study, other interesting phenomena were uncovered as well. As the temperature is decreased below ca. 120 K in certain samples, the LT phase starts to transform back to the HT phase and at 80 K the Raman spectrum becomes fairly similar to the 293 K spectrum (Figure 7). In agreement with the observations made by Moritomo et al.,[16] this LT→HT transformation at low temperatures is clearly a photoinduced effect due to the laser light used to excite Raman scattering. However, this photoinduced effect was only observed in samples **4**–**6** and **8**, but no effect was detected at all in samples **7** and **9** (Figure 6). Note also that samples **1**–**3** cannot display such phenomenon as they remain in the HT phase down to 80 K. It was established by Escax et al.[7,8] that defects play an important role in the photoconversion efficiency in Co–Fe Prussian blue analogues. In fact, vacancies provide certain flexibility to the lattice and thus allow an easier relaxation of the lattice strain induced by the volume expansion during light irradiation. However, in our case it seems difficult to find a clear link between the occurrence of the photoinduced transformation and the sample stoichiometries (see Table 1). A detailed investigation of the temperature dependence of the photoconversion efficiency and the stability of the metastable phases down to liquid helium temperatures will be necessary to determine the pertinent parameters governing this phenomenon.

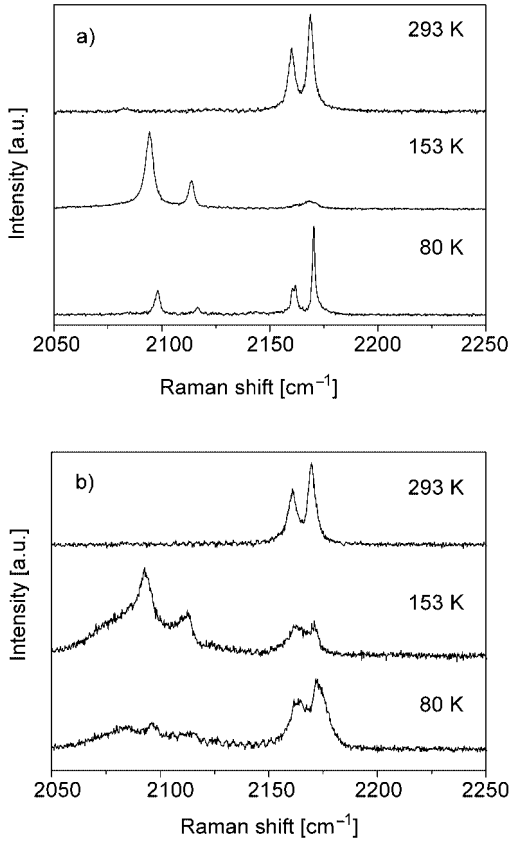

Figure 7. Raman spectra of sample **8** (a) and sample **5** (b) in the ν_{CN} frequency region at selected temperatures (cooling mode).

Figure 7 also shows that in sample **5** the Raman frequencies at low temperatures become extremely broad and unresolved. Such broadening of Raman modes can be expected as the degree of disorder increases as a result of the broader distribution in the bond lengths and the bond angles. Furthermore, as the disordered phase loses symmetry the associated selection rules may also change and one can also expect mode splittings and the appearance of modes, which are otherwise forbidden by the selection rules in the higher symmetry (i.e. more stoichiometric) forms. While in the LT phase the frequencies become badly re-

solved, the broadening of the modes in the HT phase can be used for diagnostic purposes as suggested by Vertelman et al.[11] In agreement with these authors, we observed that complexes exhibiting a conversion between the two valence-tautomeric forms show considerably narrower Raman linewidths in the CN-stretching region than complexes which do not present this phase transition (Figure 8).

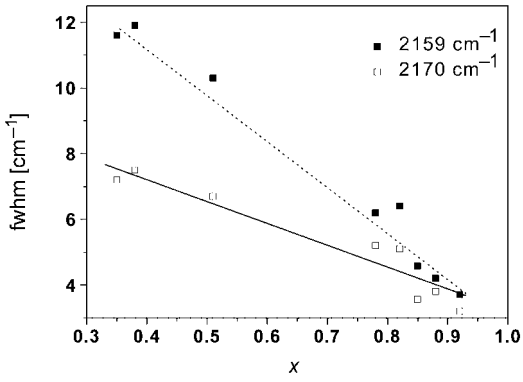

Figure 8. Full width at half maximum of selected Raman modes in $Rb_xMn[Fe(CN)_6]_y{\cdot}zH_2O$ at 298 K as a function of the Rb content. (Straight lines represent linear fits on the data.)

Conclusions

We have synthesized a series of nonstoichiometric $Rb_xMn[Fe(CN)_6]_y{\cdot}zH_2O$ compounds, some of which display charge-transfer phase-transition phenomena as a function of their composition. We have found, independently of the reaction conditions, a fairly good quantitative correlation between the Rb, Fe, and H_2O proportions, which can be explained by simple arguments based on the chemical arrangement of the system. The general tendency between the phase transition temperature and the sample stoichiometry, initially proposed by Ohkoshi et al.,[17] was confirmed. However, the quantitative correlation they propose was not observed probably because of the inherent disorder in these systems. Contrary to two independent reports,[10,21] we found that the phase transition is accompanied by an important change in the entropy of mainly vibrational origin, which is reflected in the huge changes observed in low frequency Raman spectra. Further work should address the question of the properties of the light-induced metastable phase, which was observed in the Raman spectra.

Experimental Section

Syntheses: A solution of $MnCl_2{\cdot}4H_2O$ (Aldrich) in Millipore H_2O (3 cm^3) was slowly mixed with a solution of $K_3Fe(CN)_6$ (Aldrich) and RbCl (Aldrich) in Millipore H_2O (3 cm^3). All solutions were stirred mechanically and kept at a temperature of 50 °C during the addition procedure. A brown powder precipitate was filtered, washed with Millipore H_2O and dried in air at room temperature. Nine different syntheses were realized (Table 2), six to observe the effect of concentrations (samples **1**–**6**) and three more to observe the reproducibility of the synthesis (samples **7**–**9**).

Table 2. Concentration of reactants used for the synthesis of different samples.

Sample	$MnCl_2{\cdot}4H_2O$ [mol dm^{-3}]	RbCl [mol dm^{-3}]	$K_3Fe(CN)_6$ [mol dm^{-3}]
1	0.11	0.48	0.1
2	0.14	1.01	0.1
3	0.1	2.03	0.1
4	0.06	1	0.1
5	0.11	1	0.1
6	0.07	1.02	0.1
7	0.11	1	0.1
8	0.11	1	0.1
9	0.06	1	0.1

Microanalyses: Analysis for C, H, and N were performed after combustion at 850 °C by using IR detection and gravimetry by means of a Perkin–Elmer 2400 series II device. Fe, Mn, Rb, and K concentration were determined with ICP–AES (Inductively Coupled Plasma Atomic Emission Spectroscopy) after acid digestion in H_2SO_4/HNO_3. Standard deviations of the measured metal concentrations were typically around 2 rel.%. The O and H atoms were assumed to be the only other elements present in the samples and the H_2O content was obtained by difference to 100%. (The K concentration was found to be negligible.)

Spectroscopy: Raman spectra were collected between 300 K and 80 K with a LabRAM-HR (Jobin Yvon) Raman microspectrometer and a Linkam THMS-600 cryostage. The 632.8 nm line of a He–Ne laser was used as the excitation source and a spectral resolution of ca. 1 cm^{-1} was obtained.

Magnetic Studies: Magnetic susceptibility measurements were carried out between 350–80 K by using a homemade Faraday-type magnetometer equipped with a continuous-flow Oxford Instruments cryostat. Measurements were done isothermally by steps of 10 K in 5 different magnetic fields between 4500 and 15000 Oe. Calibration of magnetic susceptibility was performed by using the reference compound $HgCo(SCN)_4$. Data were corrected for diamagnetic contributions.

Differential Scanning Calorimetry (DSC): DSC analysis was carried out with a Netsch DSC 204 instrument under helium purging gas (20 $cm^3\,min^{-1}$) at a scan rate of 10 $K\,min^{-1}$ both in heating and cooling modes. Temperature and enthalpy (ΔH) were calibrated by using the melting transition of standard materials (Hg, In, Sn). The uncertainty in the transition enthalpy (ΔH_{HL}) and entropy (ΔS_{HL}) is estimated at ca. 10% because of the subtraction of the unknown baseline and uncertainties in the residual (i.e. nontransformed) fractions.

Acknowledgments

S. Seyrac and J.-F. Meunier (LCC-CNRS) are acknowledged for CHN, DSC, and magnetic measurements. The ICP-AES analysis was made by the Service Central d'Analyse du CNRS (Vernaison).

[1] P. Gütlich, A. Hauser, H. Spiering, *Angew. Chem. Int. Ed. Engl.* **1994**, *33*, 2024.
[2] A. Bousseksou, G. Molnár, G. Matouzenko, *Eur. J. Inorg. Chem.* **2004**, 4353.
[3] D. N. Hendrickson, C. G. Pierpont, *Top. Curr. Chem.* **2004**, *234*, 63.
[4] T. Mallah, S. Thiébaut, M. Verdaguer, P. Veillet, *Science* **1993**, *262*, 1554.

[5] M. Verdaguer, A. Bleuzen, V. Marvaud, J. Vaissermann, M. Seuleiman, C. Desplanches, A. Scuiller, C. Train, R. Garde, G. Gelly, C. Lomenech, I. Roseman, P. Veillet, C. Cartier, F. Villain, *Coord. Chem. Rev.* **1999**, *190–192*, 1023.
[6] O. Sato, T. Iyoda, A. Fujishima, K. Hashimoto, *Science* **1996**, *272*, 704.
[7] V. Escax, A. Bleuzen, C. Cartier, F. Villain, A. Goujon, F. Varret, M. Verdaguer, *J. Am. Chem. Soc.* **2001**, *123*, 12536.
[8] V. Escax, A. Bleuzen, J. P. Itié, P. Munsch, F. Varret, M. Verdaguer, *J. Phys. Chem. B* **2003**, *107*, 4763.
[9] N. Shimamoto, S. Ohkoshi, O. Sato, K. Hashimoto, *Inorg. Chem.* **2002**, *41*, 678.
[10] S. Ohkoshi, H. Tokoro, K. Hashimoto, *Coord. Chem. Rev.* **2005**, *249*, 1830.
[11] E. J. M. Vertelman, E. Maccallini, D. Gournis, P. Rudolf, T. Bakas, J. Luzon, R. Broer, A. Pugzlys, T. T. A. Lummen, P. H. M. van Loosdrecht, P. J. van Koningsbruggen, *Chem. Mater.* **2006**, *18*, 1951.
[12] S. Ohkoshi, H. Tokoro, M. Utsunomiya, M. Mizuno, M. Abe, K. Hashimoto, *J. Phys. Chem. B* **2002**, *106*, 2423.
[13] H. Tokoro, S. Ohkoshi, K. Hashimoto, *Appl. Phys. Lett.* **2003**, *82*, 1245.
[14] H. Tokoro, T. Matsuda, K. Hashimoto, K. S. Ohkoshi, *J. Appl. Phys.* **2005**, *97*, 10M508.
[15] T. Yokoyama, H. Tokoro, S. Ohkoshi, K. Hashimoto, K. Okamoto, T. Ohta, *Phys. Rev. B* **2002**, *66*, 184111.
[16] Y. Moritomo, M. Hanawa, Y. Ohishi, K. Kato, M. Takata, A. Kuriki, E. Nishibori, M. Sakata, S. Ohkoshi, H. Tokoro, K. Hashimoto, *Phys. Rev. B* **2003**, *68*, 144106.
[17] S. Ohkoshi, T. Matsuda, H. Tokoro, K. Hashimoto, *Chem. Mater.* **2005**, *17*, 81.
[18] H. Tokoro, S. Miyashita, K. Hashimoto, S. Ohkoshi, *Phys. Rev. B* **2006**, *73*, 172415.
[19] M. Sorai, S. Seki, *J. Phys. Chem. Solids* **1974**, *35*, 555.
[20] S. Gawali-Salunke, F. Varret, I. Maurin, C. Enachescu, M. Malarova, K. Boukheddaden, E. Codjovi, H. Tokoro, S. Ohkoshi, K. Hashimoto, *J. Phys. Chem. B* **2005**, *109*, 8251.
[21] E. J. M. Vertelman, P. J. van Koningsbruggen at the *International Symposium on Molecular Materials based on Coordination and Organometallic Chemistry*, June 7–10th **2006**, Lyon, France.
[22] A. Bousseksou, J. Nasser, J. Linares, K. Boukheddaden, F. Varret, *J. Phys. I* **1992**, *2*, 1381.
[23] A. Bousseksou, J. J. McGarvey, F. Varret, J. A. Real, J. P. Tuchagues, A. C. Dennis, M. L. Boillot, *Chem. Phys. Lett.* **2000**, *318*, 409.
[24] S. N. Ghosh, *J. Inorg. Nucl. Chem.* **1974**, *36*, 2465.

Received: October 31, 2006
Published Online: March 6, 2007

